Int. J. Electrochem. Sci., 13 **(2018)** 362 – 372, doi: 10.20964/2018.01.32

International Journal of ELECTROCHEMICAL SCIENCE
www.electrochemsci.org

Short Communication

Effect of WO_3 Morphological Structure on its Photoelectrochemical Properties

A. S. Hammad[1,2,*], *Haitham M. El-Bery*[3], *A. H. EL-Shazly*[1] *and M. F. Elkady*[1,4]

[1]Chemical and Petrochemicals Engineering Department, Egypt-Japan University of Science and Technology, New Borg El-Arab City, Alexandria, Egypt.
[2] Chemical Engineering Department, Faculty of Engineering, Port Said University, Port Said, Egypt.
[3]Chemistry Department, Faculty of Science, Assiut University, Assiut 71516, Egypt.
[4]Fabrication Technology Department, Advanced Technology and New Materials Research Institute (ATNMRI), City of Scientific Research and Technology Applications (SRTA City), Alexandria, Egypt.
[*]E-mail: ahmed.hammad@ejust.edu.eg

Received: 18 June 2017 / *Accepted:* 27 October 2017 / *Online Published:* 1 December 2017

The influence of WO_3 morphological structure either as nanorods or nanoplates synthesized via facile hydrothermal treatment on its photoelectrochemical properties has been investigated.The morphological structure of the prepared WO_3 samples has been confirmed by TEM and SEM analysis. The average diameter of prepared WO_3 nanorods was measured to be 7nm with length up to 700 nm, while the WO_3 nanoplates were found to have a wide width up to 700 nm. The BET specific surface area of the nanoplates sample was found to be higher than that of the nanorods one with about 5 m^2 g^{-1}. The electrochemical impedance spectroscopy (EIS) measurements of the prepared WO_3 samples revealed that the nanoplates structure have lower charge transfer resistance compared with nanorods structure. These results imply that the contact between the nanoplates is better than the nanorods, which surely could enhance the conductivity and electron transfer through the material. This behavior was confirmed by the photocurrent-voltage and chronoamperometry measurements. It was indicated that the generated photocurrent by the nanoplates sample was enhanced compared with the nanorods sample giving a photocurrent density of 350 and 400 µA cm^{-2} for nanorods and nanoplates respectively. This study emphasizes on the effect of the morphological structure of WO_3 on its photo-electrochemical properties which have a high importance in photocatalytic applications.

Keywords: WO_3, Nanoparticles, Nanorods, Photocatalysis and Photoelectrochemical measurements.

1. INTRODUCTION

In the recent years, semiconductor photocatalysis gained much attention because of its ability to harness the solar energy which is considered as the most abundant power source. Many studies

investigated the idea of using active photocatalysts and sunlight in degradation of pollutants [1], water splitting [2] and CO_2 reduction [3]. To achieve a photocatalytic reaction, the semiconductor material is needed to absorb sun illumination which creates electrons and holes. Several semiconductor materials have shown their ability to conduct photocatalytic reactions such as TiO_2 [4], ZnO [5,6], and WO_3 [7]. One of the most promising materials is tungsten trioxide WO_3 which has a small band gap of approximately 2.6 eV, excellent thermal stability and resists photo-corrosion [6]. Thermal evaporation [8], chemical vapor deposition (CVD) [9, 10], hydrothermal [11], electrochemical [12], and sol-gel [13] are the common techniques to synthesize Tungsten trioxide WO_3 nanomaterials. The hydrothermal technique has a keen interest in the simple process, environmentally friendly, and mild preparation conditions [7]. In order to produce a WO_3 electrode, several techniques such as spin coating, colloidal, Electrophoretic deposition chemical and physical vapor deposition, can be used. Electrophoretic deposition (EPD) provides an easy and reliable coating technique, where charged particles suspended in solution are attracted to the electrode surface under the influence of an electric field [7]. The thickness of the formed film on the electrode is controlled by the electric field, deposition time and pH. Two types of conductive glass materials could be used in EPD processes, fluorine-doped tin oxide (FTO) and tin-doped indium oxide (ITO). The particle size and morphology of nanomaterials have a significant influence on its photoelectrochemical activity.

A lot of research has been conducted on WO_3, some studies investigated the influence of morphology on the photoelectrochemical activity of WO_3, but not all the photoelectrochemical measurements were done. Also, the effect of WO_3 morphological structure was evaluated only by the degradation of dye, but the main mechanism was not well justified with characterization results. In the present study, the influence of the shape and size of WO_3 nanostructures on the photoelectrochemical properties was investigated. Two different morphologies of WO_3 nanorods and nanoplates are synthesized by a hydrothermal process and then deposited on FTO by Electrophoretic deposition. The photocatalytic activity was evaluated by linear scan voltammetry (LSV), chronoamperometry (CAM) and electrochemical impedance spectroscopy (EIS) measurements. The physicochemical or physical and chemical properties of the prepared nanomaterials were characterized by X-ray diffraction (XRD), scanning electron microscopy (SEM), Transmission electron microscopy (TEM), Brunauer, Emmett, and Teller (BET), Fourier transform infrared (FT-IR) spectrometer.

2. EXPERIMENTAL

2.1 Materials

$Na_2WO_4 \cdot 2H_2O$ (99%), HCl (37.5%), NaCl (99%) and Iodine (≥99.99%) were purchased from Sigma-Aldrich, however, ethanol (99.5%) and acetone (≥99.5%) were purchased from Fisher Chemical. FTO-coated glass was obtained from HAGITEC CO., LTD with Rs = 7 Ω. Distilled water was used for all preparations.

2.2. Preparation procedure

2.2.1. Synthesis of WO_3 nanoplates

WO_3 nanoplates were prepared according to previously reported method [12]. Briefly, 10 g of $Na_2WO_4 \cdot 2H_2O$ was dissolved in 250 ml of distilled water. Subsequently, 3 M of HCl was added dropwise to the above solution under magnetic stirring until a yellowish precipitation was obtained. After stirring the solution for 30 min, the precipitates were collected, washed with distilled water and ethanol several times and dried at 100 ^oC. The resulted yellowish precipitate was suspended in 45 ml distilled H_2O and placed into a Teflon-lined stainless-steel autoclave. The autoclave was heated at 170 ^oC for 12 h. The prepared product was filtered, washed several times with distilled H_2O and ethanol. Finally, the powdered material was dried at 60 ◦C in air for 4 h.

2.2.2. Synthesis of WO_3 nanorods

WO_3 nanorods were prepared according to previously reported method [10]. Briefly, 2.475g of $Na_2WO_4 \cdot 2H_2O$ and 0.87g of NaCl were dissolved in 60 ml of distilled H_2O with 1:2 mole ratio respectively. After that, the pH of the solution mixture was adjusted to 2 using 3 M HCl. This solution mixture was transferred into a Teflon-lined stainless-steel autoclave and heated up to 180 ◦C and maintained for 24 h. The white precipitate was washed several times with distilled H_2O and then dried at 60 ◦C.

2.3 Characterization

The nanostructure prepared samples were characterized using SEM, TEM, FT-IR, XRD, and BET respectively. The morphology and size of the synthesized powders were observed by scanning electron microscopy (JCM-6000PLUS NeoScope Benchtop SEM) and Transmission electron microscopy (TEM, JEOL Ltd., JEM-1010). Infrared spectra were recorded using a Fourier transform infrared (FT-IR) spectrometer (Vertex 70, Bruker scientific instruments, Germany) to identify the chemical structure of the samples. X-ray diffraction was used to observe the crystalline patterns of prepared samples using (LabX XRD-6100 Shimadzu, Japan). Brunauer-Emmett Teller BET and N_2 adsorption/desorption isotherms were measured at 77 K using surface area analyzer (BelsorbminiII, BEl Japan Inc., Japan).

2.4 Photoelectrochemical measurements

Photoelectrochemical (PEC) characterizations were conducted in a single compartment cell with a Pyrex window, using a three-electrode configuration system in the presence of 0.5 M KCl electrolyte. The sample electrode WO_3 was deposited on FTO via electrophoretic deposition (EPD) as working electrode, a Pt rod as a counter electrode and an Ag/AgCl as a reference electrode. Linear scan voltammetry (LSV), Electrochemical Impedance Spectroscopy (EIS) and chronoamperometry

(CAM) were performed using a Potentiostat (Autolab Potentiostat PARSTAT 4000A). The light irradiation source of Wass ruga Seiki UV LED 365 nm with intensity up to 50 mW/cm^2 was utilized.

The powder of WO_3 nanorods and nanoplates were deposited on FTO conducting glass by EPD method for thin film fabrication. EPD was performed using 20 mg of WO_3 powder suspended in 50 ml acetone in the presence of 10 mg of iodine using ultrasonication for 5 min. Two parallel FTO electrodes (2.5 × 2 cm^2) were immersed in the solution, and 10 V of bias was applied between the electrodes for 3 min by DC power Supply (TakaSAGO ZX-400LA). The coated area was controlled to be ca. 4 cm^2 and the fabricated electrodes were dried in the air without any further treatment.

3. RESULTS AND DISCUSSION

3.1. Characterization of WO_3

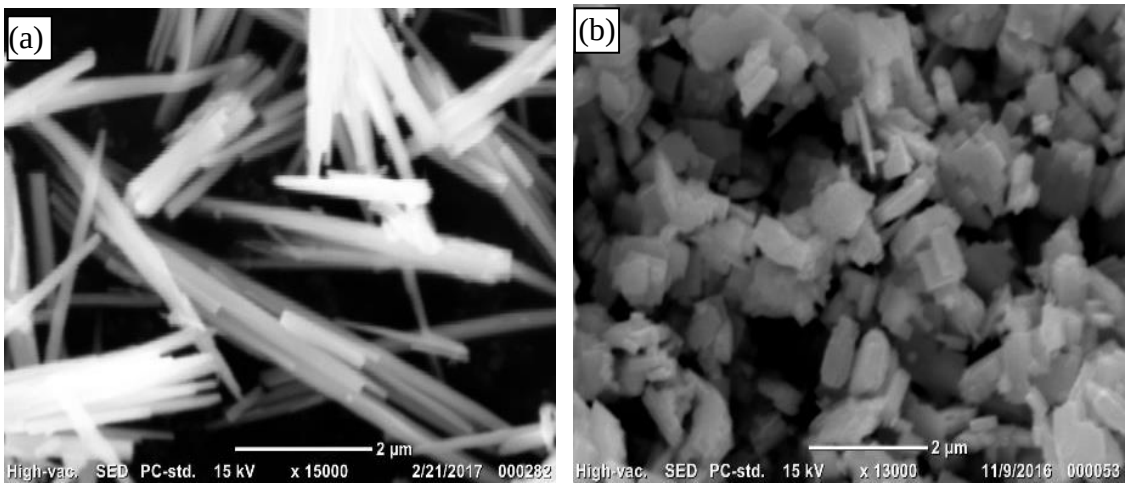

Figure 1. SEM images of (a) WO_3 nanorods, (b) WO_3 nanoplates

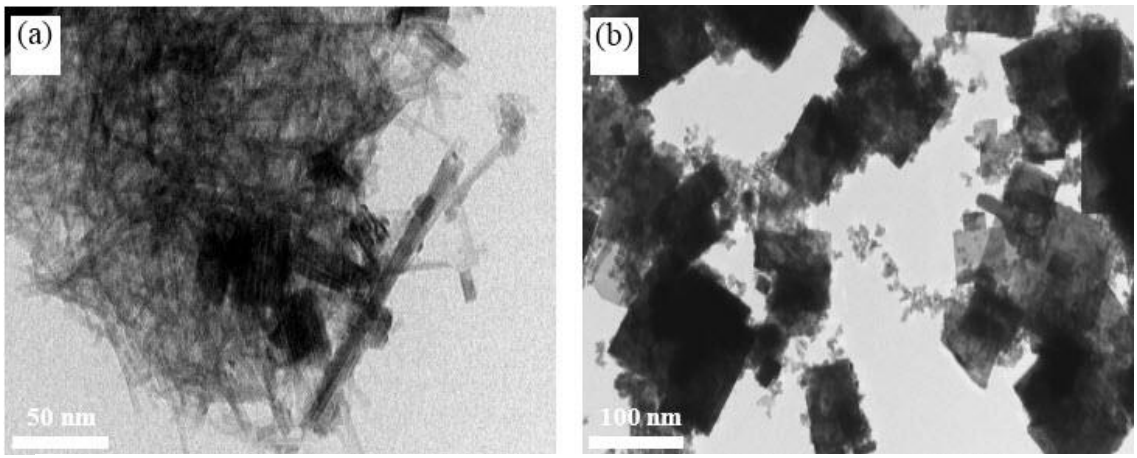

Figure 2. TEM images (a) WO_3 nanorods, (b) WO_3 nanoplates

The morphological structure of the prepared WO_3 samples was examined by SEM as shown in Fig. 1. It can be seen that the nanorods sample has a well-defined rod shape with a sharp end. Also, the WO_3 nanoplates have a nearly square morphology with sharp edges. Moreover, the TEM images (Fig. 2) reveal that the nanorods have an average diameter and length of 7 nm and 600 nm respectively. The WO_3 nanoplates have an average width of approximately 700 nm.

The BET specific surface area, pore size distribution and the N_2 adsorption/desorption isotherms of the as prepared WO_3 samples has been investigated as presented in Fig. 3. It has been found that BET surface area and pore volume of nanorods recorded 35 m^2 g^{-1} and 0.03618 cm^3g^{-1} respectively and for nanoplates are 40 m^2 g^{-1} and 0.03477 cm^3g^{-1} respectively. These results indicate that the nanoplate's morphology of WO_3 could provide higher porosity and surface area compared with that provided by nanorods morphology. This may be explained due to the nanoplates geometric shape offers more edges and faces that could effectively contribute to the total surface area.

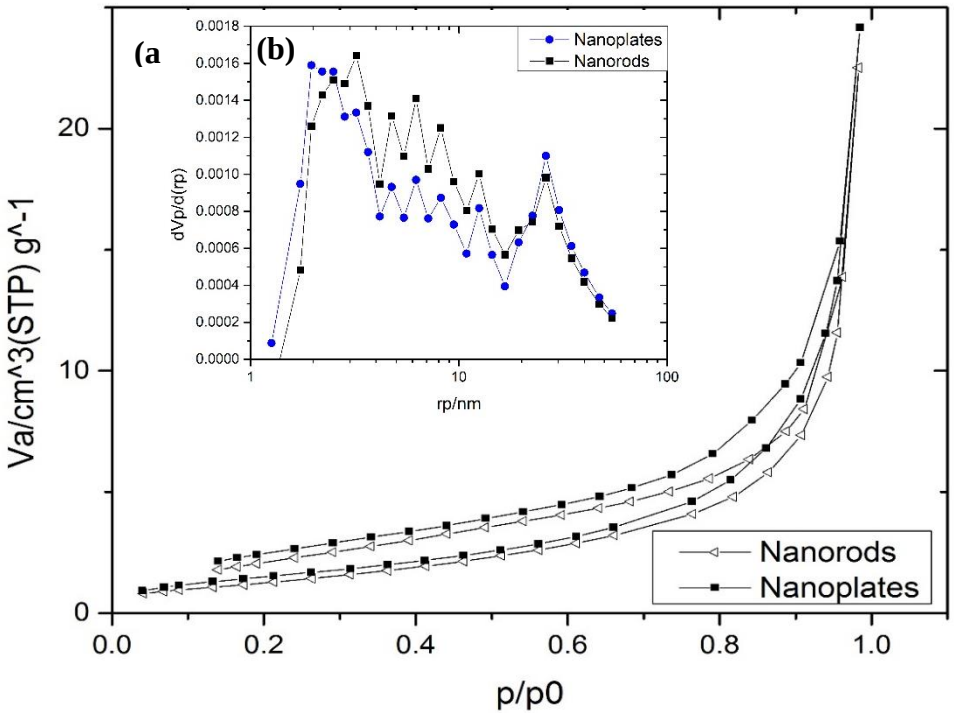

Figure 3. (a) N_2 adsorption/desorption isotherms of WO_3 samples and (b) Pore size distribution curve for prepared WO_3 samples

Furthermore, the N_2 adsorption/desorption isotherms of both WO_3 prepared samples exhibit IV isotherm type with H3 hysteresis loop typical for mesoporous materials, according to IUPAC classification [14, 15]. Fig. (3-b) indicates that the produced WO_3 structures have pore size distribution in the range from 1.2 to 54 nm.

The FTIR of synthesized WO_3 samples is shown in Fig. 4. The characteristics peaks located at 1625 and 3444 cm^{-1} are indexed to O-H bending modes of the adsorbed water. While the bands located at 728 and 817 cm^{-1} are assigned to O–W–O stretching modes.

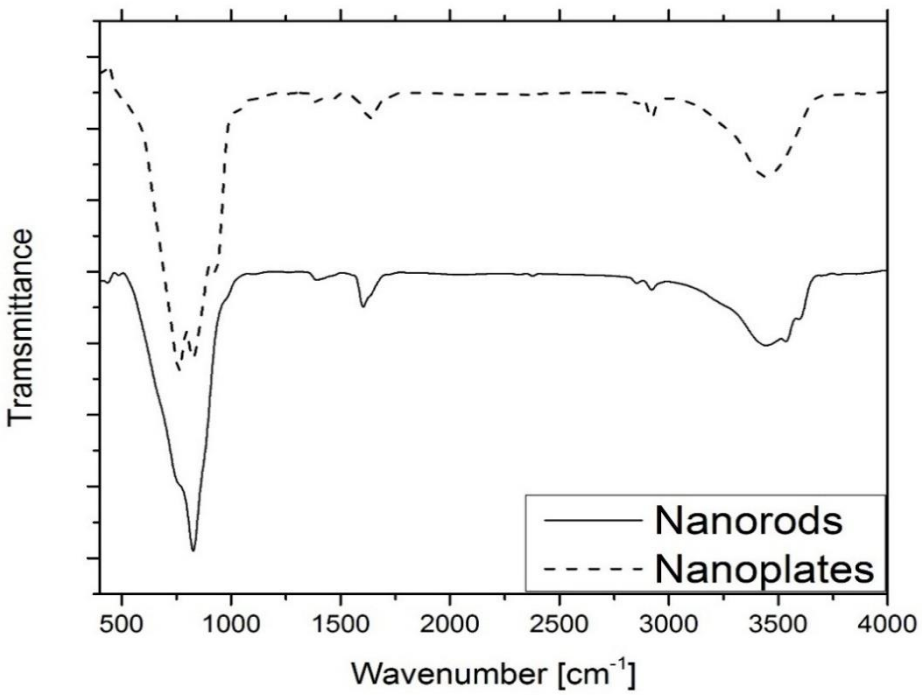

Figure 4. FTIR spectrums of prepared WO_3 in different nanorods and nanoplates morphological structure

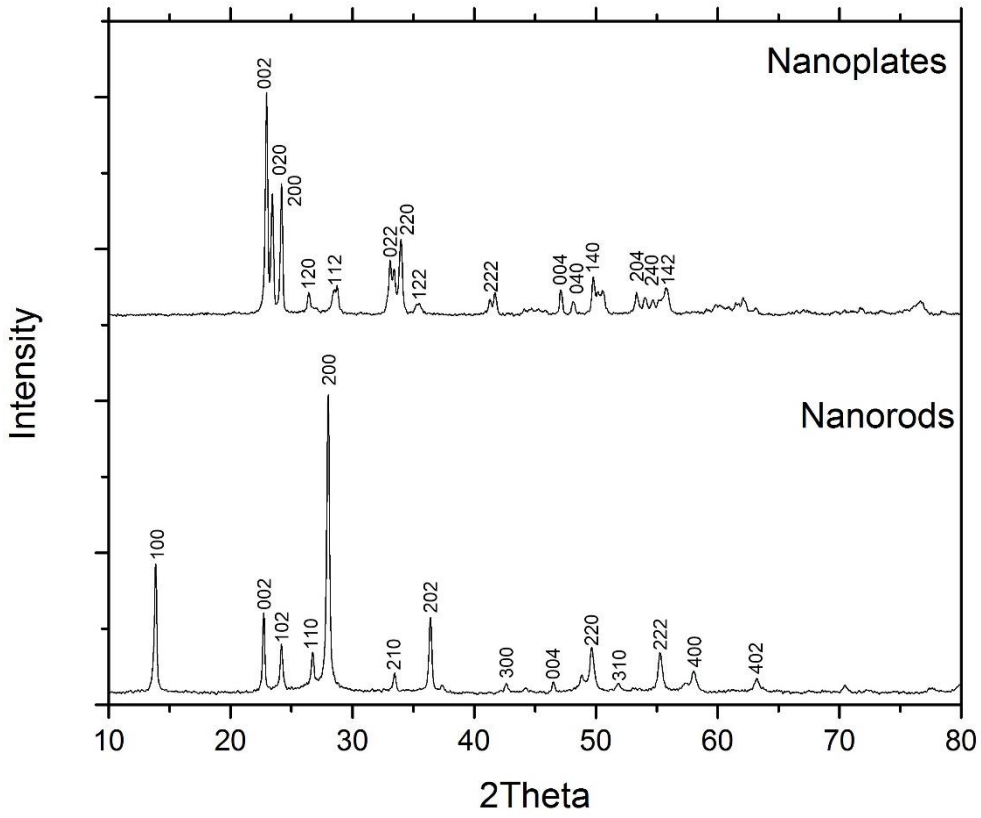

Figure 5. X-ray diffraction patterns (XRD) of prepared WO_3 in different nanorods and nanoplates morphological structure

In order to investigate the crystalline structure of prepared WO_3 samples, X-ray diffraction (XRD) measurements were implemented. X-ray diffraction patterns of prepared WO_3 samples are shown in Fig. 5. All the reflection peaks of the WO_3 nanorods sample can be readily indexed to monoclinic WO_3 (JCPDS 83-0951) and the hexagonal WO_3 (JCPDS 85-2460). While, XRD pattern of the WO_3 nanoplates, its characteristics peaks are indexed to orthorhombic phase WO_3 (JCPDS 20-1324). No diffraction peaks were observed in both WO_3 samples which indicate the purity of the prepared samples. The sharpness of diffraction peaks shows that the synthesized WO_3 has excellent crystallinity degree.

3.2. Photoelectrochemical (PEC) measurements

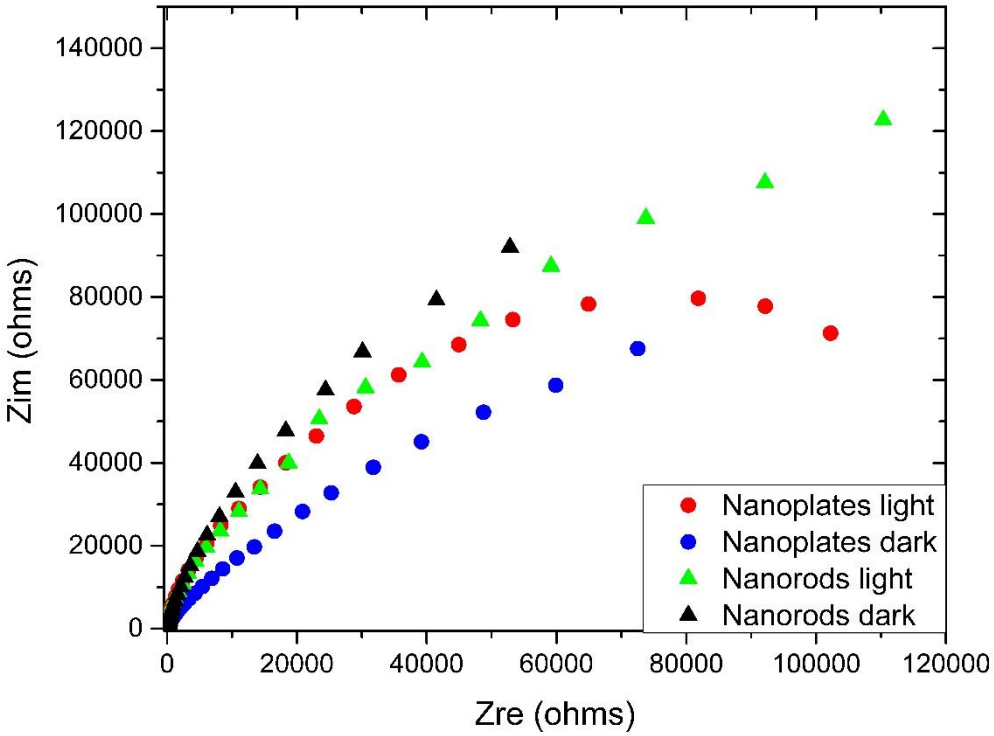

Figure 6. Electrochemical impedance spectroscopy (EIS) of WO_3 in dark and light for both nanorods and nanoplates morphological structures. Measurements were performed in a three-electrode configuration cell in 0.5 M Na_2SO_4 under UV-LED (365 nm) irradiation at a frequency range varying from 100 kHz to 0.01 Hz.

In order to evaluate the photoelectrochemical properties of WO_3 nanostructures, photoelectrochemical measurements were performed. In which photocurrent-voltage (linear scan voltammetry), chronoamperometry (CAM), and electrochemical impedance spectroscopy (EIS) were conducted inside a three-electrode configuration cell in the presence of 0.5 M Na_2SO_4 under UV-LED (365 nm) irradiation. The as prepared WO_3 samples have been deposited on the surface of FTO by EPD process.

Electrochemical impedance spectroscopy (EIS) investigates electron transfer across the electrolyte and the surface of the electrode. The measurements were held in the presence of 0.5 M Na_2SO_4 electrolyte solution at a frequency range varying from 100 kHz to 0.01 Hz in the dark and under light illumination. Fig. 6 displays the Nyquist plots of WO_3 nanorods and nanoplates samples under dark and light irradiation (λ =365 nm). The arc radius in the Nyquist plot represents layer resistance at the electrode surface. Therefore smaller arc radius implies higher charge transfer efficiency and more efficient separation of photogenerated electron-hole pairs. In both dark and light illumination, WO_3 nanoplates have smaller impedance semicircle radius compared with that of the nanorods sample. These results indicated that nanoplates sample provide a better contact between the particles that could enhance the separation and migration of the photogenerated electron-hole pairs more efficiently. WO_3 nanoplates have already reported to have smaller charge-transfer resistance compared with $WO_3 \cdot H_2O$ [16]. Previously reported studies deduced that large interfacial area between WO_3 nanoplates and electrolyte due to gaps between nanoplates, means enhanced conductivity leads to more photocurrent can be produced [17]. Also, the fabrication method of WO_3 electrode seems to have a significant impact on conductivity. For comparison, spin-coated WO_3 nanoplates film reported by Kang's group have a smaller arc than WO_3 nanoplates deposited on FTO [18].

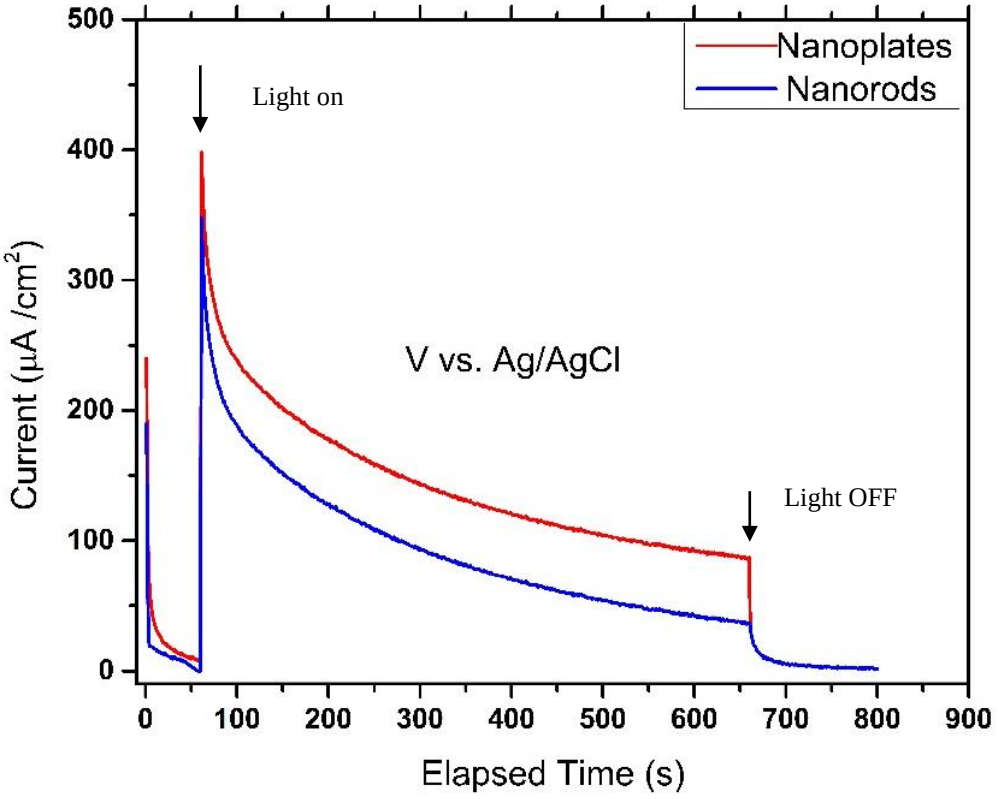

Figure 7. Chronoamperometry measurements of nanorods and nanoplates WO_3 films at 800 s (60 seconds in the dark then 600 seconds under UV-LED Light (365 nm) with maximum intensity 50 mW cm^{-2} then turned off) at À 1.17 V vs. Ag/AgCl.

Chronoamperometry measurement was conducted to determine the photocurrent stability of the WO_3 nanorods and nanoplates films as displayed in Fig.7. The test was done by applying 1.17V for 800 s for each WO_3 films. Fig.7 shows chronoamperometry curve for 800 seconds at the desired electrochemical potential, 60 seconds in the dark until a steady current was attained, then UV-LED Light (365 nm) with maximum intensity 50 mW $cm^{-2}$was used for 600 seconds and turned off. It was indicated that the two electrodes have similar curves that give a prediction that the two electrodes have the same photocurrent stability. Moreover, the WO_3 nanoplates have a relatively higher current peak at 400 mA than that of nanorods which indicate that separation and transfer of electron−hole pairs are better. Similar results were obtained in the previous study; the highest photocurrent was achieved with square platelet morphology among rod and sphere morphologies [19]. It was explained that WO_3 nanorods have a higher electron-hole recombination rate due to its morphology [20, 21]. Another explanation, WO_3 nanoplates have an orthorhombic phase which can result in increasing the photocurrent which has been studied previously [20, 22]. Although the combination of monoclinic and hexagonal phases in WO_3 nanorods seem to have a good photocurrent but the orthorhombic phase in WO_3 nanoplates provide a higher photocurrent.

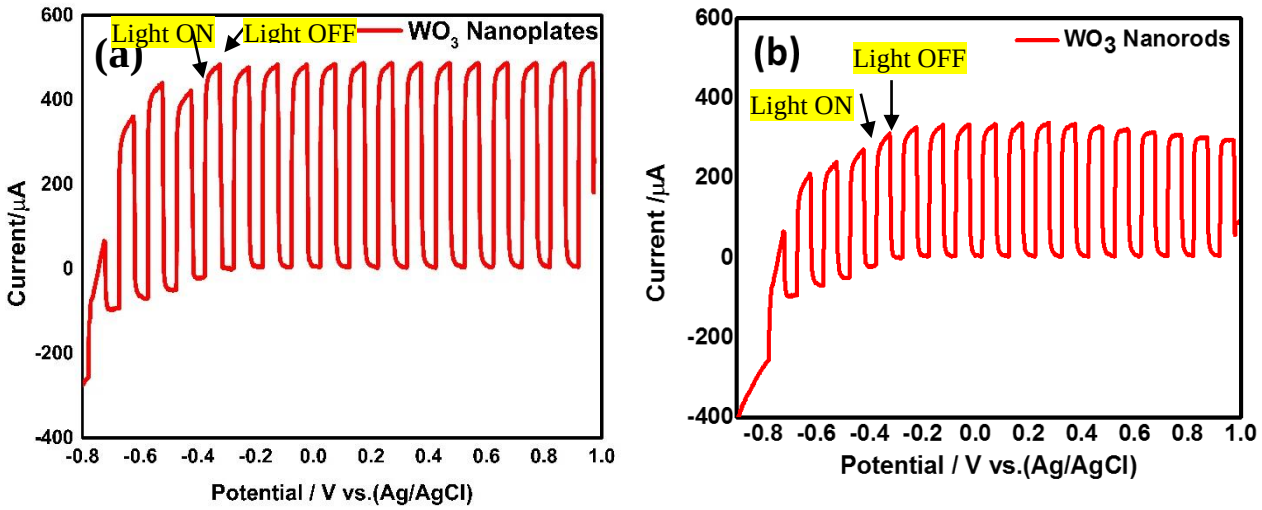

Figure 8. Linear sweep voltammograms of WO_3 in dark and light (a) nanoplates and (b) nanorods. Measurements were performed in a three-electrode configuration cell in 0.5 M Na_2SO_4 from -1 V to +1 V vs. Ag/AgCl at a scan rate of 0.05 V/s under UV-LED (365 nm) irradiation.

Linear sweep voltammetry (LSV) was used to investigate the capabilities of the WO_3 nanorods and nanoplates electrodes. The LSV was conducted from -1 V to +1 V vs. Ag/AgCl at a scan rate of 0.05 V/s under chopped light irradiation (UV-LED, 365 nm). Photocatalytic activity of semiconductor material depends on the generated amount of current due to light irradiation. The current generated due to the transfer of electrons from photoanode electrode to counter electrode upon light irradiation.

Photocurrent measurements of WO_3 nanoplates and nanorods electrodes were investigated at Fig. 8. The generation of photocurrent for the samples is observed via many on-off cycles which indicate that the electrodes are stable and the photocurrent is quite reversible.WO_3 nanoplates electrode showed about 50% higher current density compared with nanorods electrode, which stated that the separation efficiency of the electron-hole pairs significantly improved in WO_3 nanoplates sample. This is in agreement with the results discussed before in chronoamperometry results. In the previous report, nanorods showed enhanced electroactivities at −0.1 V vs. Ag/AgCl of −8.61 mA/cm^2 than that of the nanoplates (−6.67 mA/cm^2) and commercial bulk m-WO_3 (−1.08 mA/cm^2), respectively. The higher electroactivity of nanorods over nanoplates can be attributed to the higher surface area of nanorods in that study [23]. In recent study, it was found that WO_3 nanorods could not provide the best photoelectrochemical activity due to the wide band gap which reduces its ability for radiation absorbance [22, 24]. The improved photocurrent is due to highly crystalline, morphology, and higher surface area of WO_3 nanoplates, which improve light absorption [25].

4. CONCLUSIONS

In this study, WO_3 nanorods and nanoplates were synthesized via hydrothermal process to compare their photoelectrochemical properties. Two WO_3 electrodes were fabricated using electrophoretic deposition process. WO_3 nanoplates showed better photoelectrochemical properties because of their geometric shape with larger surface area and sharper edges which support the material with higher conductivity. Also, WO_3 nanoplates characterized by its low density of electron traps compared with nanorods structure material that enhances the current transfer through the electrode. The WO_3 nanoplates sample showed a real promise as photoanode for oxygen evolution reaction.

References

1. S. Nishimoto, T. Mano, Y. Kameshima and M. Miyake, *Chem. Phys. Lett.*, 500 (2010) 86.
2. C. H. Liao, C. W. Huang and J. Wu, *Catalysts.*, 2 (2012) 490.
3. J. L. White, M. F. Baruch, J. E. Pander III, Y. Hu, I. C. Fortmeyer, J. E. Park and T. W. Shaw, *Chem. Rev.*, 115 (2015) 12888.
4. K. Masaaki, K. Tsujimaru and M. Anpo, *Top.Catal.*, 49 (2008) 41.
5. K. M. Lee, C. W. Lai, K. S. Ngai and J. C. Juan, *Water Res.*, 88 (2016) 428.
6. M. F. Elkady, H. S. Hassan, *Nanoscale Res. Lett.* , 10 (2015) 474.
7. M. Yagi, S. Maruyama, K. Sone, K. Nagai and T. Norimatsu, *J. Solid State Chem.*, 181 (2008) 175.
8. M. G. Hutchins, O. Abu-Alkhair, M. M. El-Nahass and K. A. El-Hady, *Mater. Chem. Phys.*, 98 (2006) 401.
9. M. F. Elkady, H.S.Hassan, *Curr.Nanosci.*, 6 (2015), 11, 805.
10. A. H. Mahan, P. A. Parilla, K. M. Jones and A. C. Dillon, *Chem. Phys. Lett.*, 413 (2005) 88.
11. E. Khoo, P. S. Lee and J. Ma, *J. Eur. Ceram. Soc.*, 30(2010) 1139.
12. T. Todorovski and M. Najdoski, *Mater. Res. Bull.*, 42 (2007) 2025.
13. P. K. Biswas, N. C. Pramanik, M. K. Mahapatra, D. Ganguli and J. Livage, *Mater. Lett.*, 57 (2003) 4429.
14. M.Elkady, H. S. Hassan, A.Hashim, *Materials*, 9 (2016) 1.
15. J. Sungpanich, T. Thongtem and S. Thongtem, *J. Nanomater*., 131 (2014).

16. K. Ssing, D. Everett, R. Haul, L. Moscou, R. Pierotti, J. Rouquerol and T. Siemieniewsks, *Pure Appl. Chem*., 57 (1985) 603.
17. W. Li, J. Li, X. Wang, S. Luo, J. Xiao and Q. Chen, *Electrochim. Acta*, 56 (2010), 620.
18. J. Y. Zheng, G. Song, J. Hong, T. K. Van, A. U. Pawar, D. Y. Kim and Y. S. Kang, *Cryst. Growth Des*., 14 (2014), 6057.
19. W. H. Hu, G. Q. Han, B. Dong, C. G. Liu, *J. Nanomater*., 16 (2015), 23.
20. M. Rodríguez-Pérez, C. Chacón, E. Palacios-González, G. Rodríguez-Gattorno and G. Oskam, *Electrochim.Acta*., 140 (2014) 320.
21. R. H. Goncalves, L. D. Leite and E. R. Leite, *ChemSusChem*, 5 (2012), 2341.
22. M. Farhadian, P. Sangpout, and G. Hosseinzadeh, *J. Energy Chem.*, 24 (2015). 171.
23. D. J. Ham, A. Phuruangrat, S. Thongtem and J. S. Lee, *Chem. Eng. J.*, 165 (2010) 365.
24. J. Zhao, E. Olide and F. E. Osterloh, *J. Electrochem. Soc.*, 162 (2015) H65.
25. X. Feng, Y. Chen, Z. Qin, M. Wang, L. Guo, *ACS Appl. Mater. Inter.*, 8 (2016) 18089.